This article was downloaded by:
On: *16 January 2011*
Access details: *Access Details: Free Access*
Publisher *Taylor & Francis*
Informa Ltd Registered in England and Wales Registered Number: 1072954 Registered office: Mortimer House, 37-41 Mortimer Street, London W1T 3JH, UK

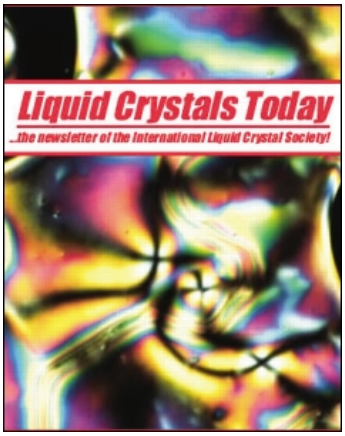


**Liquid Crystals Today**
Publication details, including instructions for authors and subscription information:
http://www.informaworld.com/smpp/title~content=t713681230

# Liquid crystalline fractals: dilatation invariant growth structures in the phase ordering process of 'banana-phases'

Ingo Dierking[a]
[a] Department of Physics and Astronomy, University of Manchester, Schuster Laboratory, Oxford Road, Manchester, UK M13 9PL; e-mail: dierking@reynolds.ph.man.ac.uk,

Online publication date: 03 December 2010

**To cite this Article** Dierking, Ingo(2003) 'Liquid crystalline fractals: dilatation invariant growth structures in the phase ordering process of 'banana-phases'', Liquid Crystals Today, 12: 1, 1 — 10
**To link to this Article: DOI:** 10.1080/14645180110000000a
**URL:** http://dx.doi.org/10.1080/14645180110000000a

PLEASE SCROLL DOWN FOR ARTICLE

Full terms and conditions of use: http://www.informaworld.com/terms-and-conditions-of-access.pdf

This article may be used for research, teaching and private study purposes. Any substantial or systematic reproduction, re-distribution, re-selling, loan or sub-licensing, systematic supply or distribution in any form to anyone is expressly forbidden.

The publisher does not give any warranty express or implied or make any representation that the contents will be complete or accurate or up to date. The accuracy of any instructions, formulae and drug doses should be independently verified with primary sources. The publisher shall not be liable for any loss, actions, claims, proceedings, demand or costs or damages whatsoever or howsoever caused arising directly or indirectly in connection with or arising out of the use of this material.

Liquid Crystals Today, 2003, Vol. 12, No. 1, 1–10

Taylor & Francis
Taylor & Francis Group

# Liquid crystalline fractals: dilatation invariant growth structures in the phase ordering process of 'banana-phases'

INGO DIERKING

Department of Physics and Astronomy, University of Manchester,
Schuster Laboratory, Oxford Road, Manchester, UK M13 9PL;
e-mail: dierking@reynolds.ph.man.ac.uk

Fractal growth structures are known to be exhibited by numerous systems in condensed matter physics, mostly forming under non-equilibrium conditions. Materials of the 'soft condensed matter' class, including colloids and polymers, are especially rich in fractal growth phenomena. It thus seems surprising that only very few reports on fractal structures in liquid crystals have been given. The likely reason is that conventional calamitic liquid crystals do not exhibit fractal growth aggregates. In contrast, the recently reported bent-core molecules, constituting the so-called liquid crystalline 'banana-phases', do in fact undergo a phase ordering process via aggregates of fractal dimensionality. In this paper the phase ordering process from the *isotropic liquid* to the *liquid crystalline* state, as well as the transition from the *liquid crystal* to the *crystalline* state, is characterized in terms of fractal dimensions of growth aggregates. Systematic investigations of the phase formation process of different 'banana-phases' as a function of time, aggregate size, cell gap, quench depth and quench rate suggest a general phase ordering process via a percolation mechanism.

## 1. Introduction

Fractals have long been known to mathematicians, but were largely disregarded until the first coherent concept of fractal geometry and its usefulness in the description of complex natural structures was triggered by the classic work of Benoit Mandelbrot [1] in the early 1980s. Since this time fractal geometry has successfully been employed in many areas of science ranging from physics, chemistry and material science all the way to biology, engineering and geology. It is particularly useful for the description of various processes of pattern formation, growth and aggregation, especially in complex and disordered systems far from equilibrium. Examples range from electro-deposition, dielectric breakdown, viscous fingering, branched growth, crack propagation or various percolation systems to retina nerve cells and growth of bacteria colonies, just to name a few. Excellent overviews have been given by Bunde and Havlin [2, 3], Vicsek [4], Meakin [5] and Kaye [6].

Growth and coarsening in the process of phase formation of condensed matter systems have long been studied experimentally as well as theoretically [7, 8], for example in condensation, crystallization, tempering of metal alloys or the phase separation of binary fluids. It has been shown that these processes generally follow simple scaling laws of the form $L(t) \sim t^n$, where $L$ is a characteristic length, $t$ the time and $n$ a universal growth exponent, which depends on the general class of systems studied (conserved order parameter (COP) or non-conserved order parameter (NCOP) systems). The phase formation processes in 'soft condensed matter', especially colloids and polymers on the other hand often lead to very complex structures, which may be described by fractal geometry and the obtained fractal dimension in turn can be related to simple generic growth models.

A classic example of such a growth model is the *diffusion limited aggregation* (DLA) model introduced by Witten and Sander [9], which describes well for example the growth of aggregates observed in electro-deposition experiments [10]. A general algorithm for respective computer simulations is as follows: (i) a seed particle is set at the origin of a lattice and (ii) a particle far from the origin performs a random walk until it meets the seed and sticks (with a certain probability) to form an aggregate. Step (ii) is repeated for many times to obtain a growing aggregate. The resultant structure is rather complex and fractal analysis yields a fractal dimension in the order of $D = 1.7$ in two-dimensional space. This model also seems to describe many aspects of dielectric breakdown, not only in gases [11], common liquids (often oils) [12, 13] or polymer foils of capacitors, but also in liquid crystal Hele–Shaw cells [14]. Note that in the model of diffusion-limited aggregation time is not defined, i.e. dynamic aspects of the aggregation process cannot be studied.

Another growth model is that of *cluster–cluster aggregation* (CCA), introduced by Meakin [15]. Here we do not set a seed particle, but rather have many particles perform a random walk simultaneously. Whenever particles meet, they stick together (again with a

*Liquid Crystals Today* ISSN 1464-5181 online © 2003 Taylor & Francis Ltd
http://www.tandf.co.uk/journals
DOI: 10.1080/14645180110000000

Downloaded At: 16:42 16 January 2011

certain probability) to form clusters which further perform a random walk until eventually all particles are part of *one* single aggregate. This model is often used to describe the aggregation of colloids [16] or, suitable as a classroom demonstration, the aggregation of wax spheres floating on water [17]. In contrast to the DLA model, here time is indeed well defined. The CCA model may also describe the formation of the loosely cross-linked polymer beads observed in some polymer-stabilised liquid crystals (PSLCs) for monomer concentrations close or above the solubility limit [18]. The fractal dimension of CCA clusters generally varies between $D = 1.6$ and 1.8, depending on the sticking probability and other details of the employed computer simulation.

Finally, *percolation* models account for a variety of different growth structures [19, 20], ranging from systems like ink spreading in absorbing paper, water being pushed through compressed sand, or the spread of epidemics and forest fires. The growth model involves (i) setting a seed particle at the origin of a lattice with all nearest neighbours being 'alive', i.e. being lattice sites which can be occupied; (ii) the 'alive' sites are occupied with a probability $p$ which are then part of the growing cluster, or 'killed' with a probability $1 - p$; (iii) the new nearest neighbours are then 'alive' and steps (ii) and (iii) are repeated many times to form a growing aggregate. Two-dimensional percolation clusters at the percolation threshold, i.e. clusters spanning throughout the whole sample, have a fractal dimension in the order of $D = 1.9$ ($D = 1.89$ from theory). Growth is governed by local interactions. An example from liquid crystal research may be the formation of polymer networks by photopolymerisation of reactive monomers in PSCTs at concentrations well below the solubility limit [18].

Having given a variety of examples for fractal growth structures in different soft matter materials and their respective generic growth models, it seems surprising that only very few reports have been published that relate fractal geometry to liquid crystals. One such report gave an estimation of the fractal dimension of a single dendritic-like texture of a discotic columnar hexagonal phase [21], but no investigations concerning the actual growth process were carried out. Saffman–Taylor instabilities [22] in liquid crystal Hele–Shaw cells exhibit similar patterns for viscous fingering [23–25], although these structures are not related to a phase ordering process. Other investigations describe fractally homogeneous distributions of nuclei [26, 27] and topological defects [28, 29] in nematic liquid crystals during phase ordering and coarsening, respectively. This paper presents a summary of detailed investigations into the fractal aspects of liquid crystal phase ordering in bent-core molecules.

## 2. Experimental

Subjecting a conventional calamitic liquid crystal to a rapid temperature quench below the clearing point, i.e. a quench from the isotropic phase into the liquid crystal temperature range, results in a metastable situation at isothermal conditions with the high temperature isotropic phase having a larger free energy $F$ than the low temperature liquid crystal phase. Due to thermal fluctuations liquid crystalline nuclei are formed, which grow spontaneously once a critical nucleus radius is exceeded. In the case of the isotropic to nematic or cholesteric transition, these nuclei are often spherical as shown in figure 1 (*a*). For the isotropic to smectic transition the well-known bâtonnets are usually observed, as exemplarily depicted in the texture photograph of figure 1 (*b*). In both cases the individual aggregates exhibit a Euclidean dimension of $D = 2$ in two-dimensional space. (Most phase-ordering experiments with liquid crystals in sandwich cells can effectively be regarded as being two-dimensional, because the cell gap of the order

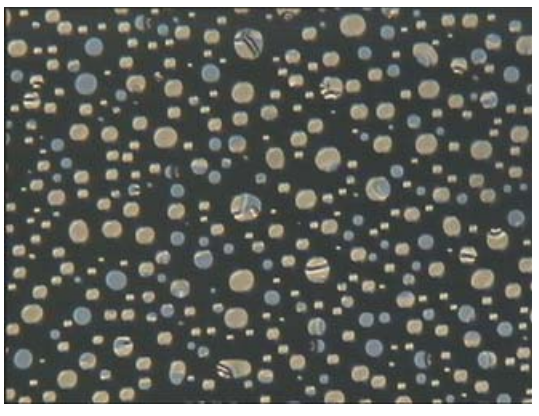

(*a*)

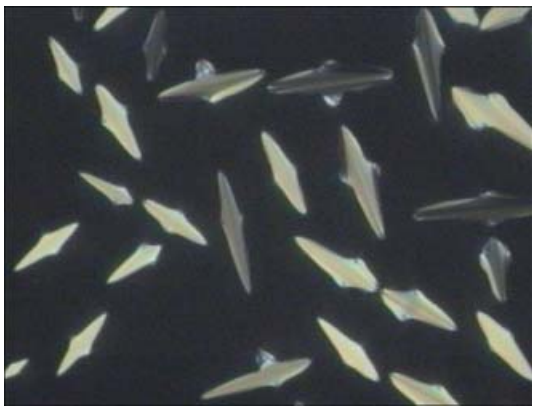

(*b*)

Figure 1. Growth patterns of conventional calamitic liquid crystals: (a) at the isotropic to cholesteric and (b) at the isotropic to smectic A transition. (The textures are reproduced from: Dierking, I., 2003, *Textures of Liquid Crystals* (Weinheim: Wiley-VCH).)

Downloaded At: 16:42 16 January 2011

of a few micrometres is much smaller than the growing nucleus, while the cell extension in perpendicular directions can be regarded as infinite.) The growth process of the nematic/cholesteric spherical nuclei can be described by the above-mentioned universal growth law $L(t) \sim t^n$ [30, 31] with $L$ representing the nucleus diameter. Experimentally, the growth exponent is found to be $n = 1/2$ for vanishing quench depth (thus $\Delta F \approx 0$) and approaching $n = 1$ for large quench depths [32–34], in accordance with theoretical predictions [8, 35]. The growth of smectic bâtonnets is obviously anisotropic, but choosing the long and the short bâtonnet axis as a characteristic length $L$, it has been shown that these still follow the above universal growth laws [36].

The phase-ordering process of the 'banana' liquid crystal phases is *qualitatively* different. We do not observe nuclei of a regular geometric shape as those of the calamitic phases (figure 1), but rather complex structures, growth aggregates of very irregular shape (figure 2), which suggest a description by methods of fractal geometry, as was also noted in [37].

The compound investigated is that of the first bent-core mesogen reported by Sekine *et al.* [38], which has the structural formula shown below:

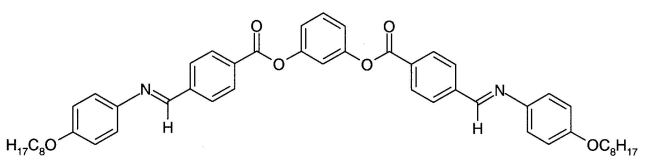


For the studies presented here the phase-transition temperatures were determined by polarising microscopy (Nikon OPTIPHOT2-POL, Leitz Orthoplan) on very slow cooling (Mettler FP52, FP82 hot stages) in commercially available sandwich cells (E.H.C, Japan) of varying thickness. The phase sequence in °C is given by Iso. 169 B2 150 B3 145 B4 (with B4 being a crystalline phase). Transition temperatures were slightly dependent on cell gap and the compound showed a two-phase region of approximately 3 K at the isotropic to liquid crystal transition, which is quite common for bent-core mesogens and may be attributed to impurities. Two separate phase-ordering processes were investigated: the *isotropic* to *liquid crystal* B2 transition and the *liquid crystal* B3 to *crystal* B4 transition. All measurements reported below were reduced to the respective phase-transition temperature by introducing the quench depth $\Delta T$ as a relevant parameter. The isotropic–B2 transition temperature was taken as the temperature at which the first liquid crystalline nuclei were observed on very slow cooling, while the B3–B4 transition is rather sharp. The accuracy of relative temperatures is estimated to be better than 0.1 K.

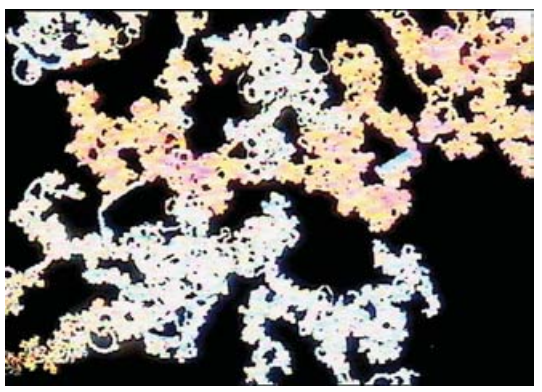

Figure 2. Typical texture of a banana B2 phase growing from the isotropic melt.

For the investigations of the isotropic–B2 phase ordering process, digital images were recorded by a microscope-mounted video camera (Sony Hyper HAD model SSC-DC38P) at an image size of 768 × 576 pixels, corresponding to a sample size of 1080 μm × 820 μm. The general experimental conditions were chosen as follows: cell gap $d = 3\,\mu m$, quench depth $\Delta T = 0.3$ K and quench rate $R = 3$ K min$^{-1}$. The results for the different investigation series presented below were obtained by varying only the respective parameter, leaving other conditions unchanged. For the B3–B4 transition, images were recorded at a resolution of 720 × 540 pixels, corresponding to a sample size of 640 μm × 490 μm. Experimental conditions were as follows: cell gap $d = 2\,\mu m$, quench depth $\Delta T = 0.5$ K and quench rate $R = 3$ K min$^{-1}$. Specific parameters were changed for the each of the different investigations undertaken.

Time-dependent fractal dimensional analysis was carried out with BENOIT 1.3 from TruSoft International. Several different methods were employed, which all gave comparable values for the fractal dimensions.

1. *The box dimension method.* The fractal dimension $D_b$ is defined as the exponent in the proportionality

$$N(d) \sim \frac{1}{d^{D_b}} \tag{1}$$

with $N(d)$ as the number of occupied boxes of side length $d$ being occupied by the data set. An illustrative example is depicted in figure 3(*a*) for a single growth aggregate, giving a fractal box dimension of $D_b = 1.86$. For a Euclidean object like a sphere or a square, equation (1) gives $D_b = 2$.

2. *The information dimension method.* This method is very similar to the box dimension method, except that the information dimension method weights the occupied boxes according to their object pixel content. The fractal dimension $D_i$ is defined from the proportionality

$$I(d) \sim -D_i \log(d) \tag{2}$$

Downloaded At: 16:42 16 January 2011

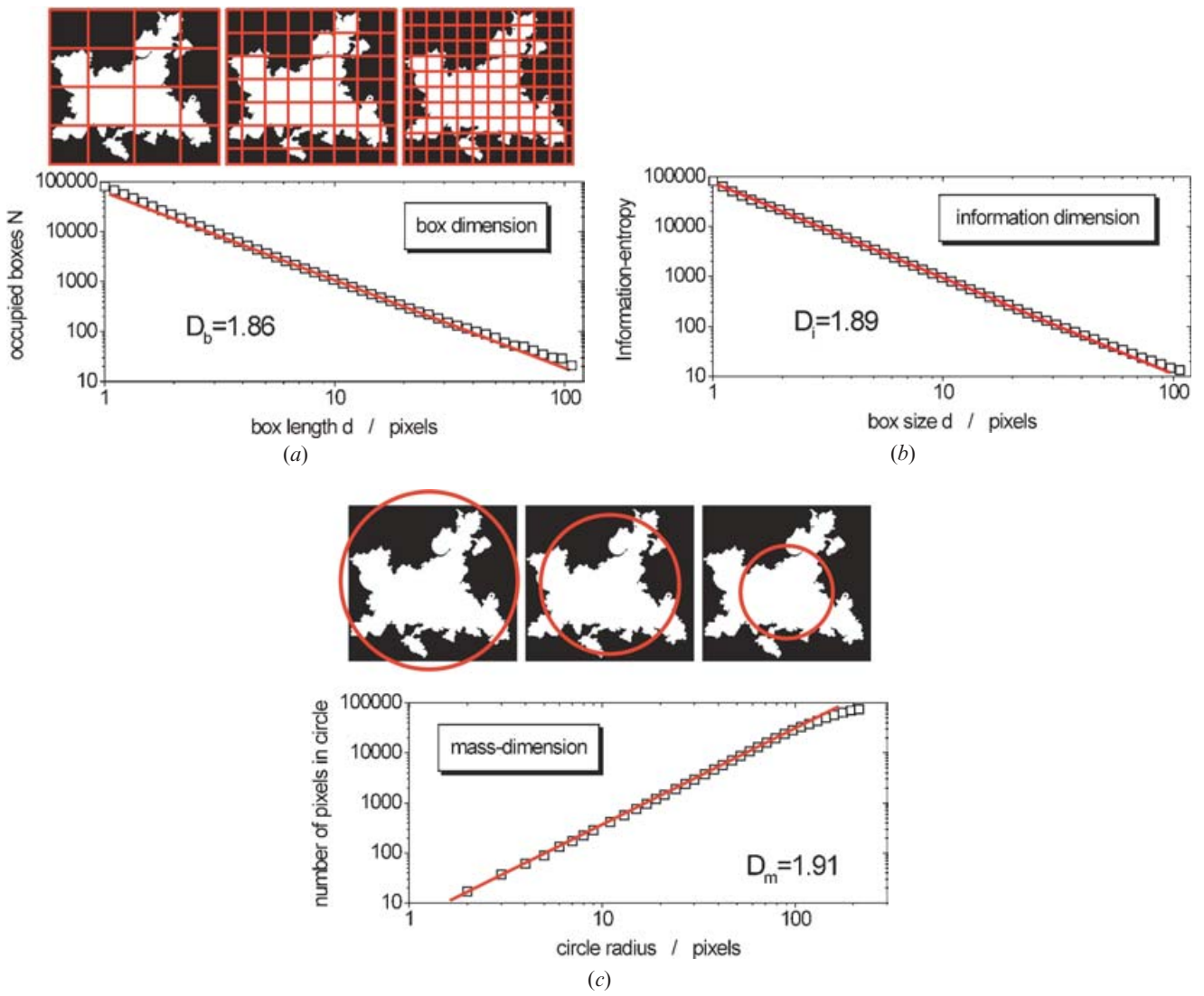


Figure 3. Illustration of the application of methods to determine fractal dimensions related to the covered cluster areas of objects: (a) the box dimension method giving $D_b$ (equation (1)); (b) the information dimension method giving $D_i$ (equation (2)); and (c) the mass dimension method giving $D_m$ (equation (4)).

with

$$I(d) = -\sum_{i=1}^{N(d)} m_i \log(m_i) \tag{3}$$

where $m_i = M_i/M$, with $M_i$ the number of points in the $i$th box and $M$ the number of total points in the data set.

Generally $D_i \geqslant D_b$ and the quality of the digital image being analysed can be judged by the difference between $D_b$ and $D_i$. If the image contains a large number of 'stray pixels', $D_b$ may be (considerably) smaller than $D_i$ (by a factor of up to $\Delta D \approx 0.1$) and in this case the information dimension method provides the more reliable results. The method is demonstrated in figure 3 (*b*), analysing the same single aggregate as above and $D_i = 1.89$ is obtained. Again, a Euclidean object would give a fractal dimension of $D_i = 2$.

3. *The mass dimension method.* This method is often employed for radially symmetric objects (as in dielectric breakdown). The fractal dimension $D_m$ is defined from the proportionality

$$m(r) \sim r^{D_m} \tag{4}$$

with $m(r) = M(r)/M$ the 'mass' within a circle of radius $r$, where $M(r)$ is the data set points contained within a circle and $M$ the total number of points in the set. In the ideal (mathematical) case $D_m = D_b$. The mass dimension method is employed in figure 3 (*c*) for the same aggregate as above, and yields $D_m = 1.91$.

Downloaded At: 16:42 16 January 2011

The time-resolved fractal analysis of liquid crystalline B2 growth aggregates forming from the isotropic melt was in each case carried out by minimization of the standard deviation SD of a linear fit to a log–log plot according to equations (1), (2) and (4) to SD $< 0.001$. For each image the box, respectively radius size, was varied over more than two orders of magnitude, resulting in variations of the dependent variable over more than four orders of magnitude. The linear regime from which the fractal dimensions were determined covered at least one order of magnitude in box or radius size. For reasons of clarity, the results given below represent the average ($D_{\mathrm{avg}}$) of the three fractal dimensions $D_{\mathrm{b}}$, $D_i$ and $D_m$ with the error bars indicating the range of confidence.

The above fractal dimensions are related to the covered cluster area, the so-called 'mass' of an object. For the studies related to the liquid crystal to crystal transition (B3–B4), we also investigated single growing aggregates ('islands' or 'closed loops'), for which further fractal dimensions can be determined, which are related to the perimeter of the cluster. These are as follows.

4. *The area–perimeter method*. This relates the area $A$ of a closed loop to its perimeter $P$ by the dimension $D_{\mathrm{p}}$, which is defined from the proportionality

$$A \sim P^{2/\mathrm{D}_p} \tag{5}$$

An illustrative example of this method is shown in figure 4 (*a*) for the above single aggregate, giving $D_{\mathrm{p}} = 1.53$. Euclidean objects have a dimension of $D_{\mathrm{p}} = 1$.

5. *The ruler method*. The ruler dimension $D_{\mathrm{r}}$ is related solely to the perimeter of an object. It is defined from the proportionality

$$M(l) \sim l^{-D_r} \tag{6}$$

with $M(l)$ being the number of steps a ruler of length $l$ has to be taken around the perimeter of an object, which has to be a closed loop. The ruler method is demonstrated in figure 4 (*b*) and gives $D_{\mathrm{r}} = 1.27$ for the above aggregate. If the perimeter is Euclidean, the ruler dimension is $D_{\mathrm{r}} = 1$. Also the latter two fractal dimensions were determined by minimization of the standard deviation of a linear fit to a log–log plot to SD $< 0.001$.

## 3. Experimental results and discussion

This paper summarizes results obtained from the investigations of isothermal growth of aggregates of a low-temperature phase after a rapid temperature quench below the phase-transition temperature from a high-temperature phase of bent-core molecules. This is namely the liquid to liquid crystal transition (iso.–B2) and the liquid crystal to crystal transition (B3–B4). For a more detailed account of the investigations the reader is referred to references [39–42].

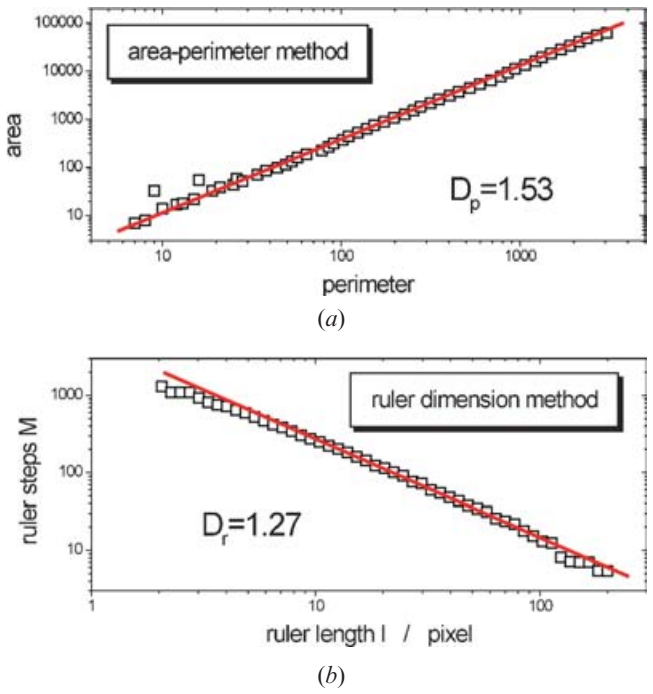


Figure 4. Illustrations of the application of (a) the area–perimeter dimension method and (b) the ruler dimension method to determine the fractal dimensions related to the perimeter of an object resembling a closed loop yielding $D_{\mathrm{p}}$ (equation (5)) and $D_{\mathrm{r}}$ (equation (6)), respectively.

### 3.1. *The isotropic–liquid crystal B2 transition*

The first phase-ordering process studied is that from the isotropic to the liquid crystal B2 phase, of which an example is given in supplemental video 1† (note that the video merely illustrates the growth process and that it does not represent its real time dynamics). In the video 'white' (birefringent) liquid crystal aggregates are growing within the sea of the 'black' isotropic phase. When investigating fractal growth phenomena, it first has to be shown that the structures studied do in fact exhibit dilatation or scale invariance. This is demonstrated in figure 5, where five aggregates of different size, ranging from approximately 50 to 1100 μm (the whole texture), were analysed with respect to their fractal dimensions by methods 1 through 3. The average fractal dimension $D_{\mathrm{avg}}$ for all aggregates is practically constant, thus demonstrating dilatation invariance over more than one order of magnitude in cluster size. Note that for this investigation the phase-ordering process was not completed ($t \approx 20$ s) and that the fractal dimensions given are not the saturation values. The actual time development of the fractal dimension during the isothermal phase-ordering process is depicted in figure 6 for an analysis of the whole texture image. A sharp increase of

† Please see the Supplemental Materials section to download this video.

Downloaded At: 16:42 16 January 2011

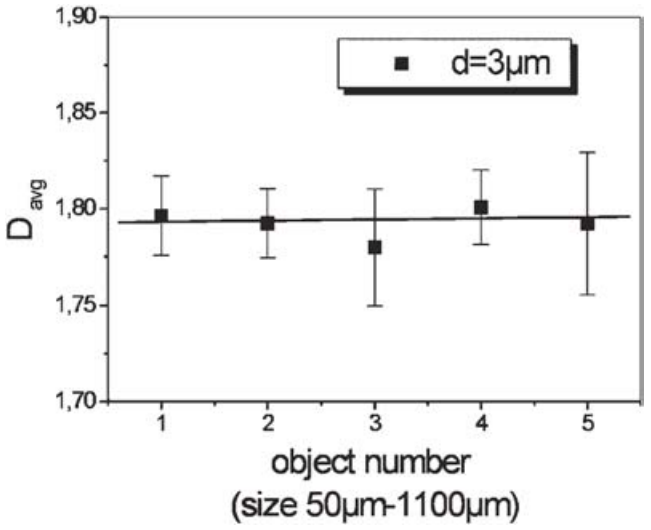


Figure 5. Average fractal dimension $D_{avg}$ for five different growth aggregates in the size range between 50 and 1100 µm (whole texture), illustrating self-similarity.

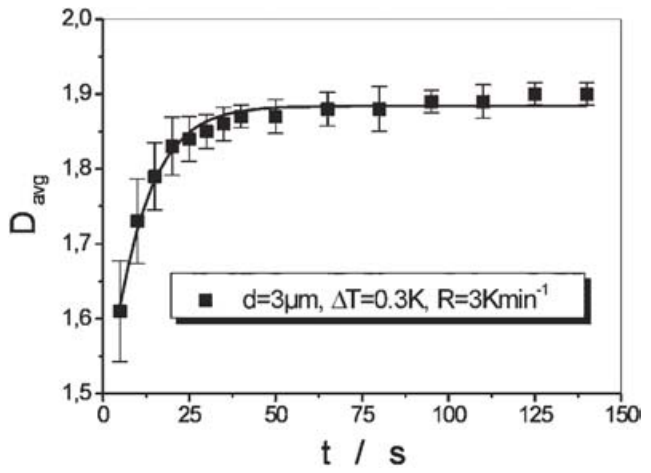


Figure 6. Time development of the average fractal dimension $D_{avg}$ during the B2 phase-ordering process.

the average fractal dimension is observed for short times up to approximately $t \approx 30$ s, which then quickly saturates at a value of $D_{avg} = 1.9$, clearly smaller than $D = 2$, as would be expected for Euclidean clusters. While the saturation value of the fractal dimension hints towards percolation at the percolation threshold, the dynamics of the phase-ordering process may indicate a growth process changing from below the percolation threshold at short times ($D \approx 1.6$) to one at the percolation threshold ($D = 1.9$) in the long time limit. For such a crossover, two-dimensional percolation theory predicts a change in the fractal dimension from $D = 1.56$ to $D = 1.89$ [19]. It is further worthwhile to point out that different clusters have the same fractal dimension, which stays constant and does not change even during coalescence [40].

Let us now examine the dependence of the average fractal dimension $D_{avg}$ of growth aggregates on various parameters of the phase-ordering process, namely the quench depth $\Delta T$ and the quench rate $R$, but especially also the dependence on sandwich cell gap $d$, in order to clarify whether fractal growth is an *intrinsic* property of banana-phases, or if it is just a surface-mediated effect, induced by interactions between the liquid crystal and the substrates of the cell. The latter is an interesting question, because it is well known that banana-phases exhibit great resistance to any of the common orientation techniques employed for calamitic nematic or smectic liquid crystals. This includes planar as well as homeotropic anchoring conditions, temperature cycling and temperature gradients, electric field treatments, mechanical shear or combinations thereof.

Figure 7 (*a*) shows the dependence of the saturation value of the average fractal dimension $D_{avg}$ as a function of quench depth $\Delta T$. This is found to be basically independent of quench depth at a value of $D_{avg} = 1.88$, possibly only slightly decreasing with increasing quench depth. For quench depths larger than $\Delta T > 0.6$ K isothermal growth could no longer be assured. A more detailed description of the time dependence of the box dimension $D_b$ as well as the quench depth dependence of the box dimension $D_b$, the information dimension $D_i$ and the mass dimension $D_m$ can be found in reference [40].

Also the quench rate $R$, i.e. the rate of temperature change to reach a certain quench depth, has no influence on the saturation value of the average fractal dimension obtained, which is again found to be in the order of $D_{avg} = 1.89$ (figure 7 (*b*)). This is behaviour that one would intuitively expect, because the actual phase-ordering process still proceeds under isothermal conditions. For quench rates larger than $R > 10$ K min$^{-1}$ the passive cooling of the used hot stages no longer allowed reliable measurements to be obtained under isothermal conditions. Again, time-dependent measurements and details for different fractal dimension methods can be found in reference [40].

Finally, figure 7 (*c*) depicts the cell gap dependence of the saturation values of the average fractal dimension $D_{avg}$ obtained from methods 1 to 3. The average fractal dimension is found to increase from $D_{avg} = 1.83$ for small cell gaps of $d = 2$ µm to $D_{avg} = 1.9$ for large cell gaps of $d = 15$ µm. In the $D_{avg}(d)$ dependence, saturation behaviour can be observed for cell gaps larger than approximately $d > 6$ µm. This can be attributed to a vanishing influence of the substrates on the liquid crystal phase ordering process. The saturation cell gap of

Downloaded At: 16:42 16 January 2011

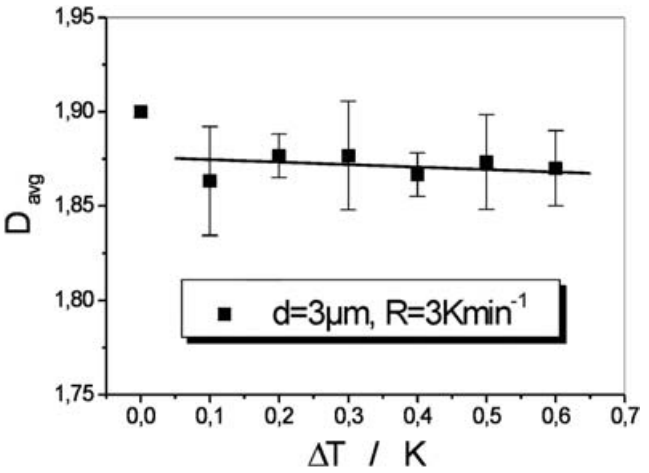


(*a*)

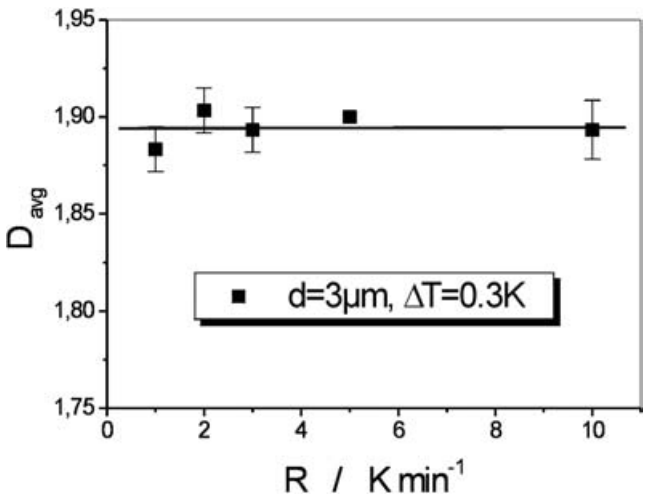


(*b*)

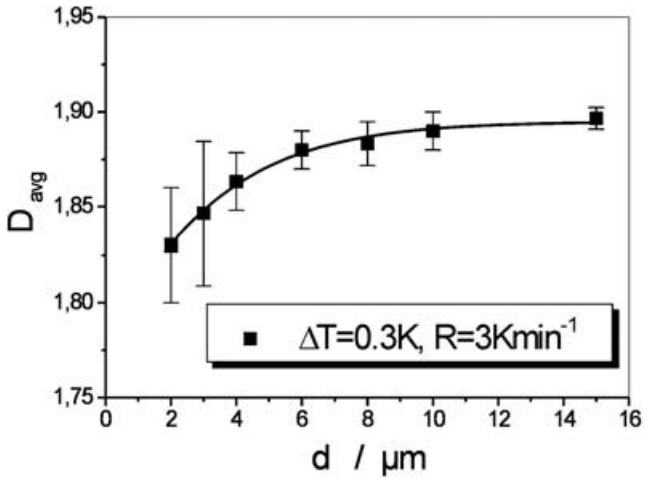


(*c*)

Figure 7. Dependence of the average fractal dimension $D_{avg}$ for the isotropic to B2 phase ordering process on (a) quench depth $\Delta T$, (b) quench rate $R$ and (c) cell gap $d$.

$d \approx 6\,\mu m$ is of the same order as is commonly observed for many other measurements of liquid crystal material parameters, indicating the sample dimension where surface-dominated behaviour crosses over to bulk behaviour. We note that even for much larger cell gaps, i.e. true bulk material, an average fractal dimension clearly smaller than $D = 2$ is obtained. This means that the fractal growth structures observed for banana phases are not surface-induced, but that fractal growth is indeed an intrinsic property of liquid crystal phases formed from bent-core molecules. This may account for the poor ability of these materials to be oriented uniformly by any of the common orientation methods. For time-dependent investigations on the cell gap dependence of the fractal dimensions we again refer to reference [40]. It is interesting to note that for decreasing cell gaps confinement effects seem to play an increasing role in the phase-ordering process, which is also observed for common calamitic phases [43, 44]. More detailed studies concerning this behaviour are currently being carried out.

The growth of the liquid crystal B2 phase from the isotropic melt is accomplished via the formation of only very few nuclei. These grow in a complex fashion, undergo coalescence with proceeding time and in the long time limit lead to aggregates which span throughout the whole sample area. For illustration figure 8 shows an exemplary binary texture image where the red area was produced with one single area colour fill (by use of standard image software). This behaviour, together with the determined average fractal dimensions in the order of $D_{avg} \approx 1.89$, being largely independent of the varied external parameters such as quench depth $\Delta T$, quench rate $R$ or sample dimension $d$ (for bulk samples), suggests that the phase-ordering process of the B2 phase does in fact represent a percolation system at the percolation threshold (in the saturation limit). On the molecular level the driving mechanism for percolation growth of the B2 phase may be related to a combination of steric effects and interactions between the local spontaneous

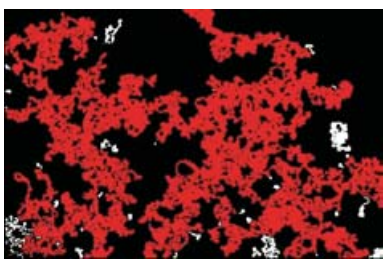

Figure 8. Late time texture image of a growing B2 liquid crystal cluster, illustrating a percolation system at the percolation threshold by its fractal dimension of $D = 1.9$ and a cluster that spans throughout the whole sample area (red).

Downloaded At: 16:42 16 January 2011

polarization vectors. At this point we can not give a molecular model, which will generate a macroscopic banana-phase percolation cluster, i.e. it is not yet clear how local interactions are related to the probability of site occupation in the percolation model, but respective simulations will be carried out in due time.

### 3.2. *The liquid crystal B3–crystal B4 transition*

Let us now turn to the crystallization of the same bent-core mesogen as discussed above, i.e. the transition from the liquid crystalline B3 to the crystal B4 phase. The growth process of the crystal B4 phase is faster than that of the liquid crystalline B2 phase and is illustrated in supplemental video 2.‡ As explained above for video 1, this video does not represent the real time dynamics of the phase-ordering process, but is merely meant to serve as an illustrative example. The growth process of the crystalline B4 phase can be observed between crossed polarizers as dark B4 areas growing from the 'sea' of the birefringent, bright liquid crystal phase. For the following investigations it is worthwhile stressing the point mentioned above concerning the reliability of results obtained from different methods of fractal dimension determination. As can be seen in supplemental video 2, a relatively large number of 'stray pixels' (not being part of a growing aggregate) are observed in the digital, binary texture images. These lead to errors in the determined fractal dimensions, which can be quite substantial in the case of the *box dimension method*, but are considerably smaller for the *information dimension method* and the *mass dimension method*. This will become apparent from the results presented below, keeping in mind that for ideal objects we should obtain $D_\mathrm{b} = D_m$ and $D_\mathrm{i} \geqslant D_\mathrm{b}$. The $D_\mathrm{b}$ values are included in the figures presented below, only to illustrate that the very popular and often employed box dimension method may *not* give reliable results for *all* experimental situations, even though a small standard deviation of a linear fit (on a log–log scale) might be obtained. In the following, we will limit our presentation of experimental results for the crystallization process to those obtained on single growth aggregates. Further data for an analysis of whole textures can be found in reference [41].

Figure 9 (*a*) depicts the time development of the fractal dimensions related to the covered area of the B4 growth aggregate, namely the box dimension $D_\mathrm{b}$ (squares), the information dimension $D_i$ (circles) and the mass dimension $D_m$ (up triangles). In all cases the fractal dimension quickly reaches saturation, but relating to our discussion above, we note that $D_i$ and $D_m$ exhibit approximately equal values, while $D_\mathrm{b}$ is considerably smaller, due to errors caused by the 'stray pixels'. An average saturation value of the information dimension and the mass dimension is obtained as $D_\mathrm{avg} = 1.9$ and we note that this is equivalent to the dimensions obtained for the liquid crystalline B2 phase, which we related to a percolation system. Investigating a single aggregate, i.e. a closed loop or an 'island', we can also employ fractal dimension methods related to the perimeter of the growth aggregate (figure 9 (*b*)), namely the determination of the area–perimeter dimension $D_\mathrm{p}$ (down triangles) and the ruler dimension $D_\mathrm{r}$ (diamonds). For Euclidean objects both of these dimensions should be equal to 1. This is clearly not the case as demonstrated in figure 9 (*b*) with $D_\mathrm{p} \approx 1.35$ and $D_\mathrm{r} \approx 1.25$ and we can conclude that also the perimeter of the crystal B4 aggregates shows fractal growth features.

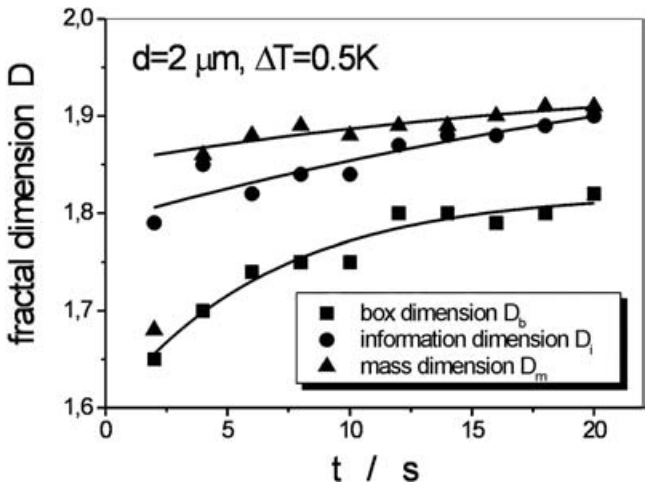


(*a*)

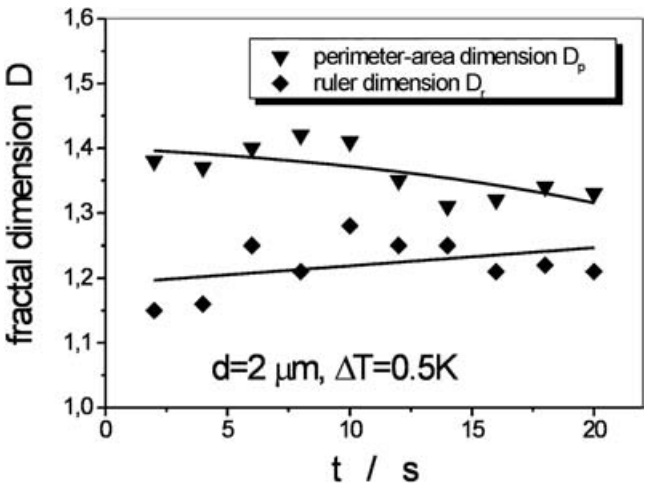


(*b*)

Figure 9. Time development of fractal dimensions (a) $D_\mathrm{b}$, $D_i$ and $D_m$, related to covered cluster area and (b) $D_\mathrm{p}$ and $D_\mathrm{r}$, related to the cluster perimeter for the B4 crystallization process.

‡ Please see the Supplemental Materials section to download this video.

Downloaded At: 16:42 16 January 2011

Variation of the quench depth $\Delta T$ does not have any significant influence on the crystal growth structures, as demonstrated in figure 10. Figure 10 (*a*) depicts the quench depth dependence of the fractal dimensions related to the covered area of the growth aggregate ($D_b$: squares, $D_i$: circles and $D_m$: up triangles, with values of $D_b$ being too small due to stray pixels), while figure 10 (*b*) shows those related to the perimeter of a single aggregate ($D_p$: down triangles and $D_r$: diamonds). Again, we find an average value of the information dimension and the mass dimension of $D_{avg} = 1.9$ while $D_p \approx 1.35$ and $D_r \approx 1.25$.

Figure 11 depicts the cell gap dependence of fractal dimensions determined by various methods up to a cell gap of $d = 6\,\mu m$. For larger substrate spacing the crystallization process does not proceed in two dimensions and

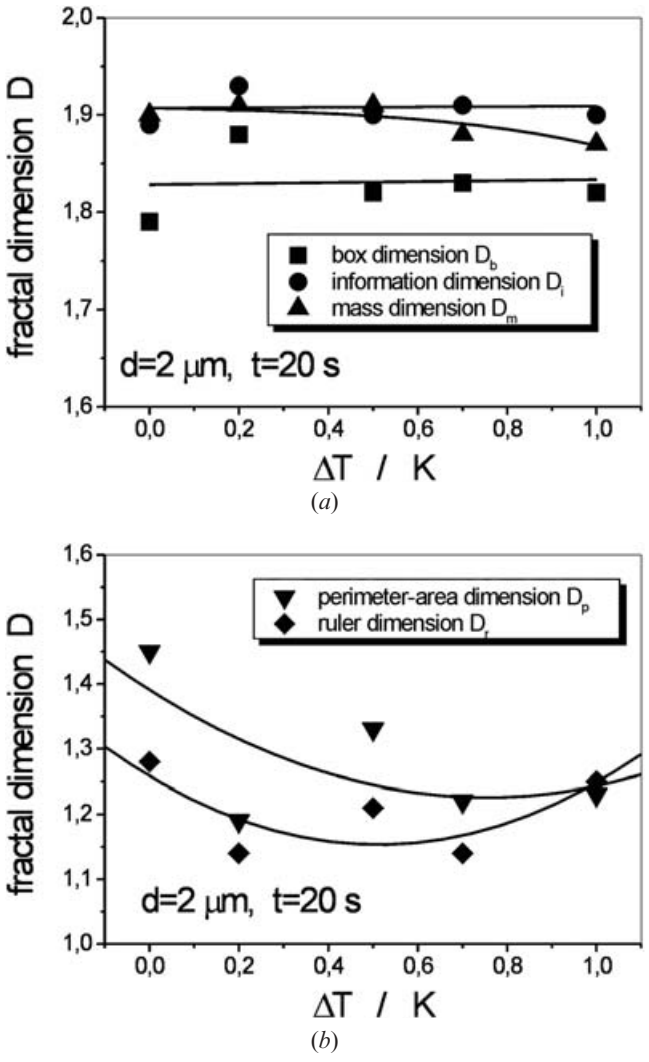


(*a*) (*b*)

Figure 10. Quench depth dependence of fractal dimensions (a) $D_b$, $D_i$ and $D_m$, related to covered cluster area and (b) $D_p$ and $D_r$, related to the cluster perimeter for the B4 crystallization process.




(*a*) (*b*)

Figure 11. Cell gap dependence of fractal dimensions (a) $D_b$, $D_i$ and $D_m$, related to covered cluster area and (b) $D_p$ and $D_r$, related to the cluster perimeter for the B4 crystallization process.

the crystal clusters are not uniformly black. This means that these textures cannot be used for a fractal analysis, because they cannot unambiguously be converted to binary digital images. Figure 11 (*a*) shows the cell gap dependence of the fractal dimensions related to the covered area of a single growth aggregate. An average dimension obtained from the information and the mass method gives $D_{avg} \approx 1.88$ for $d = 6\,\mu m$, while again $D_p \approx 1.35$ and $D_r \approx 1.25$ (figure 11 (*b*)). The crystallization process is accomplished much faster for increasing cell gap and time-dependent fractal dimensional data can be found in reference [41].

Also for the phase-ordering process from the liquid crystalline to the crystal state, fractal growth aggregates can be observed, which in the late time limit basically

Downloaded At: 16:42 16 January 2011

form a single cluster spanning the whole sample. Fractal dimensions related to the covered cluster area are found to be in the order of $D_{avg} \approx 1.9$, suggesting growth via a percolation mechanism, similar to the observations for the isotropic to liquid crystal B2 transition. An analysis of single growth aggregates by methods related to the perimeter of a cluster yields fractal dimensions, which are clearly larger than $D = 1$ and indicate that not only the covered area but also the perimeter of the aggregates exhibits dilatation invariance during isothermal growth.

## 4. Conclusions

Fractal growth is a commonly observed feature in soft matter materials, which has long been disregarded in the study of liquid crystals. In this paper we have summarized our investigations on the isothermal phase-ordering process of 'banana-phases' after a temperature quench across transitions from the isotropic to liquid crystal phase as well as the liquid crystal to crystalline phase. We have unambiguously demonstrated fractal growth patterns in liquid crystals and given a detailed and systematic account of the development of fractal dimensions obtained by a variety of different methods as a function of time, cluster size, quench depth, quench rate and sample dimension. Considering the actual growth process as observed in polarizing microscopy, together with the fractal dimensions determined, the phase ordering of bent-core molecules is intrinsically accomplished via non-Euclidean, fractal aggregates and is most likely related to a percolation mechanism. Experimental evidence was given that in the long time limit (at saturation of the fractal dimension) the phase-ordering process of banana phases represents the first liquid crystal example of a percolation system at the percolation threshold. Future efforts will be directed towards the identification of a molecular model generating a percolation mechanism, which will lead to macroscopic growth structures like those observed in the experiments presented above, with comparable fractal dimensions.

## References


[1] Mandelbrot, B., 1982, *The Fractal Geometry of Nature* (San Francisco: Freeman).
[2] Bunde, A., and Havlin, S. (editors), 1994, *Fractals in Science* (Berlin: Springer).
[3] Bunde, A., and Havlin, S. (editors), 1996, *Fractals and Disordered Systems* (Berlin: Springer).
[4] Vicsek, T., 1989, *Fractal Growth Phenomena* (Singapore: World Scientific).
[5] Meakin, P., 1998, *Fractals, Scaling and Growth Far from Equilibrium* (Cambridge: Cambridge University Press).
[6] Kaye, B. H., 1994, *A Random Walk Through Fractal Dimensions*, 2nd edn (Weinheim: VCH).
[7] Ratke, L., and Voorhees, P. W., 2002, *Growth and Coarsening* (Berlin: Springer).
[8] Bray, A. J., 1994, *Adv. Phys.*, **43,** 357.
[9] Witten, T. A., and Sander, L. M., 1981, *Phys. Rev. Lett.*, **47,** 1400.
[10] Matsushita, M., Sano, M., Hayakawa, Y., Honjo, H., and Sawada, Y., 1984, *Phys. Rev. Lett.*, **53,** 286.
[11] Niemeyer, L., Pietronero, L., and Wiesmann, H. J., 1984, *Phys. Rev. Lett.*, **52,** 1033.
[12] Lam, L., Freimuth, R. D., and Lakkaraju, H. S., 1991, *Mol. Cryst. Liq. Cryst.*, **199,** 249.
[13] Sheu, C.-R., Cheng, C.-Y., Wang, P.-S., Lee, C.-Y., and Pan, R.-P., 2000, *Chin. J. Phys.*, **38,** 461.
[14] Dierking, I., 2001, *J. Phys. D: Appl. Phys.*, **34,** 806.
[15] Meakin, P., 1983, *Phys. Rev. Lett.*, **51,** 1119.
[16] Weitz, D. A., and Oliveria, M., 1984, *Phys. Rev. Lett.*, **52,** 1433.
[17] Daoud, M., and van Damme, H., 1999, chapter 2. In *Soft Matter Physics*, edited by M. Daoud and C. E. Williams (Berlin: Springer). The authors refer to an experiment by C. Allain and M. Cloitre, published in popular form in *Pour la Science*, April 1993.
[18] Dierking, I., 2002, *J. Phys. D: Appl. Phys.*, **35,** 2520.
[19] Stauffer, D., and Aharony, A., 1992, *Introduction to Percolation Theory* (London: Taylor & Francis).
[20] Sahimi, M., 1994, *Applications of Percolation Theory* (London: Taylor & Francis).
[21] Baehr, C., Ebert, M., Frick, G., and Wendorff, J. H., 1990, *Liq. Cryst.*, **7,** 601.
[22] Saffman, P. G., and Taylor, G. I., 1958, *Proc. Roy. Soc.*, **A245,** 312.
[23] Buka, A., Kertész, J., and Vicsek, T., 1986, *Nature*, **323,** 424.
[24] Horvath, V. K., Kertész, J., and Vicsek, T., 1987, *Europhys. Lett.*, **4,** 1133.
[25] Buka, A., Pulffy-Muhoray, P., and Racz, Z., 1987, *Phys. Rev. A*, **36,** 3984.
[26] Nakagawa, M., Kobayashi, K., Hori, M., Okabe, M., and Hori, Y., 1991, *Mol. Cryst. Liq. Cryst.*, **195,** 15.
[27] Dierking, I., 2001, *Europhys. Lett.*, **55,** 40.
[28] Massalska-Arodz, M., 1994, *Nukleonika*, **39,** 77.
[29] Massalska-Arodz, M., 1998, *Acta Phys. Pol. A*, **94,** 41.
[30] Lifshitz, I. M., 1962, *Sov. Phys. JETP*, **15,** 939.
[31] Allen, S. M., and Cahn, J. W., 1979, *Acta Metall.*, **27,** 1085.
[32] Diekmann, K., Schumacher, M., and Stegemeyer, H., 1998, *Liq. Cryst.*, **25,** 349.
[33] Dierking, I., 2000, *J. Phys. Chem. B*, **104,** 10 642.
[34] Dierking, I., 2001, *Appl. Phys. A*, **72,** 307.
[35] Bray, A. J., 1993, *Physica A*, **193,** 41.
[36] Dierking, I., and Russell, C., 2003, *Physica B*, **325,** 281.
[37] Thisayukta, J., Nakayama, Y., Kawauchi, S., Takezoe, H., and Watanabe, J., 2000, *J. Am. Chem. Soc.*, **122,** 7441.
[38] Sekine, T., Niori, T., Sone, M., Watanabe, J., Choi, S. W., Takanishi, Y., and Takezoe, H., 1997, *Jpn. J. Appl. Phys.*, **36,** 6455.
[39] Dierking, I, 2001, *CHEMPHYSCHEM*, **2,** 59.
[40] Dierking, I, 2001, *J. Phys.: Condens. Matter*, **13,** 1353.
[41] Dierking, I, 2001, *Physica B*, **304,** 51.
[42] Dierking, I., Sawade, H., and Heppke, G., 2001, *Liq. Cryst.*, **28,** 1767.
[43] Dierking, I., Ghosh, A. K., and Haase, W., 2002, *J. Phys.: Condens. Matter*, **14,** 13441.
[44] Dierking, I., unpublished results.


Downloaded At: 16:42 16 January 2011